Journal of Photochemistry and Photobiology A: Chemistry 213 (2010) 129–135

Contents lists available at ScienceDirect

Journal of Photochemistry and Photobiology A: Chemistry

journal homepage: www.elsevier.com/locate/jphotochem

Influence of nitrogen chemical states on photocatalytic activities of nitrogen-doped TiO_2 nanoparticles under visible light

Sangwook Lee[a], In-Sun Cho[a], Duk Kyu Lee[a], Dong Wook Kim[a], Tae Hoon Noh[a], Chae Hyun Kwak[a], Sangbaek Park[a], Kug Sun Hong[a,*], Jung-Kun Lee[b], Hyun Suk Jung[c]

[a] School of Materials Science and Engineering, Seoul National University, San 56-1, Shillim-dong, Kwanak-gu, Seoul 151-744, South Korea
[b] Department of Mechanical Engineering and Materials Science, University of Pittsburgh, Pittsburgh, PA 15260, USA
[c] School of Advanced Materials Engineering, Kookmin University, Jeongneung-dong, Seongbuk-gu, Seoul 136-702, South Korea

ARTICLE INFO

Article history:
Received 21 January 2010
Received in revised form 6 May 2010
Accepted 23 May 2010
Available online 31 May 2010

Keywords:
Nitrogen-doped TiO_2
Chemical states
XPS
Visible light
Photocatalyst

ABSTRACT

Nitrogen-doped TiO_2 (N-TiO_2) nanoparticles with a homogeneous anatase structure were synthesized using three different chemical methods. X-ray photoelectron spectra (XPS) analysis shows that nitrogen was successfully doped into TiO_2 nanoparticles and the nitrogen atoms are present in both substitutional and interstitial sites. The electron binding energy (BE) of N 1s core level is found to depend on the synthesis methods. Changes in Ti–O bond lengths of the substitutional and interstitial N doped-TiO_2 were calculated by computational geometry optimization, and confirmed by Raman shift analysis. Differences in UV–vis light absorption and visible-light-induced photocatalytic activity of three N-TiO_2 samples were attributed to their different nitrogen states within TiO_2 lattice, which would create different defect levels. The defect levels were confirmed by photoluminescence (PL) analysis and density of states (DOSs) calculation. From one to one correspondence between XP spectrum and photocatalytic activities, it is concluded that nitrogen atoms in substitutional sites enhances the photocatalysis of TiO_2 under visible light more effectively than nitrogen atoms in interstitial sites.

1. Introduction

Photocatalysts that are sensitive to visible light have attracted much attention for their potential use of solar energy [1–4]. In particular, nitrogen-doped TiO_2 is known to be a promising visible-light photocatalyst [2]. Therefore, there have been a number of studies on the synthesis and characterization of various types of N-doped TiO_2, including thin films [2,5–7], single crystals [8–10], and powders [1,4,11–17].

However, the chemical states of doped N and its relation to photocatalytic properties under visible light are still controversial. Saha and Tompkins [18] and Asahi et al. [2] measured the N 1s core levels using XPS analysis and observed three peak structures at binding energies of 402, 400, and 396 eV. They assigned the peaks as atomic β-N (396 eV) and molecularly chemisorbed γ-N_2 (400 and 402 eV) [2,18]. Also, Asahi et al. [2] concluded that the active sites of N for photocatalysis under visible light are the substitutional sites, which correspond to the peak at 396 eV in the XP spectra. Thereafter, Irie et al. [19] observed N 1s peak at 396 eV and explained it to result from a substitutional N in O–Ti–N. Diwald et al. [9] observed the N 1s feature at 396.7 eV and assigned the peak to N_2^- anion replacing oxygen in the TiO_2 lattice. In contrast to these studies, there have been also a great number of reports showing that the signal at around 396 eV is completely absent in N-TiO_2 [4,12,17,20–27]. Burda and co-workers [4,20,24] found that the binding energy of N 1s extended from 397.4 eV to 403.7 eV and was centered at 401.3 eV, and they assigned the peak to partially oxidized N in N–Ti–O linkages. They reported that the synthesized N-TiO_2 nanoparticles had photocatalytic activity in the visible light region [4]. Thereafter, Sathish et al. [17] and Ma et al. [28] found the N 1s core level to be at 398.2 eV and 398.3 eV, respectively. They explained these peaks in terms of nitrogen in N–Ti–O linkages (nitrogen is substituted for oxygen in the initial O–Ti–O structure), and Sathish et al. [17] reported that the N-TiO_2 exhibited photocatalytic activity under the visible light region. A few researchers have reported that the photocatalytic power of N-TiO_2 under visible light is correlated with the N 1s core level peak at around 400 eV [2,9,12,18,23,26,28]. In some of these reports, molecularly adsorbed or interstitially doped N species such as NO and NH_x [1,9,29,30], were proposed to generate the peak at around 400 eV in the XP spectrum and develop the photoactive properties under the visible light.

As stated above, the chemical states of nitrogen and their effects on the photocatalytic activity in the visible light are still controversial. It may be due to the fact that the N doping is very sensitive

* Corresponding author. Tel.: +82 2 880 8024; fax: +82 2 886 4156.
E-mail addresses: kshongss@plaza.snu.ac.kr (K.S. Hong), jul37@pitt.edu (J.-K. Lee), hjung@kookmin.ac.kr (H.S. Jung).

1010-6030/$ – see front matter © 2010 Elsevier B.V. All rights reserved.
doi:10.1016/j.jphotochem.2010.05.011

processing conditions. Therefore, previous studies observed only part of chemical states of N allowed in TiO_2. In the present work, N-TiO_2 samples that were synthesized by different methods show that the N 1s binding energy can be 398.3, 401.5, and 400 eV, depending on the processing conditions. This is the first investigation reporting the N 1s binding energy of both 398.3 and 401.5 eV and the effect of N doping states on the photocatalytic properties of N-TiO_2 nanoparticles. The doping states of nitrogen (i.e. substitutional or interstitial) with different binding energy N-TiO_2 were analyzed by combining experimental and theoretical studies. In addition, the effects of the N doping states on the optical properties and photocatalytic activity of N-TiO_2 in the visible region were investigated.

2. Experiment

2.1. Preparation of nanoparticles, films, and photoelectrochemical (PEC) cells

Bare-TiO_2 nanoparticles were synthesized via the hydrolysis of titanium tetraisopropoxide (TTIP, $Ti(OC_3H_7)_4$, 97%, Aldrich Chemicals Co.) with excess water ($[H_2O]$:[Ti] = 50:1) at 80 °C. The sol was stirred at 80 °C for 24 h and dried at 90 °C in an oven. The dried powder was annealed at 450 °C for 1 h in air, and the resultant white powder was denoted as "PT". The three different types of N-TiO_2 nanoparticles called "NT1", "NT2", and "NT3" were prepared by the following methods. NT1 nanoparticles were prepared by annealing the PT powder at 400 °C for 2 h in flowing NH_3 gas. NT2 nanoparticles were synthesized by the hydrolysis of TTIP with NH_4OH solution ($[NH_4OH]$:$[H_2O]$:[Ti] = 5:45:1) at 80 °C. The sol was stirred for 24 h, centrifuged, and then washed with distilled water five times; the subsequent drying and annealing process was identical to that used for PT. NT3 nanoparticles were synthesized by hydrolysis of titanium chloride (100 mL, 2 M $TiCl_4$ in H_2O) with ammonium hydroxide (900 mL, 5 M NH_4OH in H_2O) at room temperature. The suspension was stirred for 2 h, centrifuged, and then washed with distilled water five times; the subsequent drying and annealing process was identical to that used for PT. The resultant NT1, NT2, and NT3 powders were pale yellow. TiO_2 films were prepared using the synthesized nanoparticles. Dried nanoparticles were dispersed in a mixture of water, ethanol, and acetyl acetone, and then spin-coated on fused silica substrates. The spin-coated films were annealed using the several methods (PT, NT1, NT2, and NT3) described above. The thicknesses of the films were measured using a field-emission scanning electron microscope (FESEM, model JSM-6330F, JEOL, Japan) and all of films were about 1 μm thick.

2.2. Characterization

The crystal structures of the prepared samples were characterized using a powder X-ray diffractometer (XRD, model M18XHF-SRA, MAC-Science Instruments, Japan). The morphologies of the prepared TiO_2 nanoparticles were observed using a high-resolution transmission electron microscope (HRTEM, model JEM 3000F, JEOL, Japan). The chemical states of N in TiO_2 were analyzed using X-ray photoelectron spectroscopy (XPS, model SIGMA PROBE, ThermoVG, UK). The XP spectra were acquired using monochromatic Al–K radiation (100 W), and the core levels of N 1s were calibrated with respect to the C 1s level at 284.5 eV. The diffuse reflectance spectra were obtained using a UV–vis-NIR spectrophotometer (model U-3501, Hitachi, Japan) and were converted to the absorbance spectra by the Kubelka–Munk method. The photoluminescence (PL) spectra of the samples were obtained using a photoluminescence spectrometer (SPEX 1403, SPEX). The specific surface areas of the TiO_2 nanoparticles were measured using a Brunauer–Emmett–Teller (BET) analyzer (BELSORP-mini II, BEL, Japan). The Raman spectra were recorded using a Raman spectrometer (T64000, HORIABA Jobin Yvon, France).

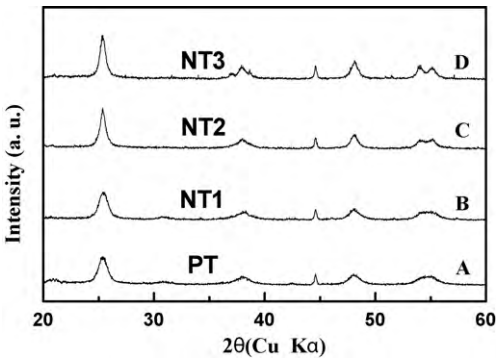

Fig. 1. Powder X-ray diffraction patterns.

2.3. Evaluation of photocatalytic activity and computational geometry optimization

The photocatalytic activities of the prepared powders were evaluated by measuring the decomposition of phenol (10 ppm) in an aqueous system. The catalyst (0.1 g) was added to 100 mL of phenol solution in a Pyrex reactor. Prior to irradiation, the suspension was stirred in the dark until the concentration of solution was stabilized. A 200 W halogen lamp was used as a light source and a 420-nm cut-off filter was employed to filter UV light and excite samples only by visible light. The concentration of the phenol solution was measured using the UV–vis spectrophotometer. Moreover, the amount of total oraganic carbon (TOC) in the aqueous solution was measured by Total Organic Carbon analyzer (5310C, Sievers, U.S.A.). In addition to the powders, we also examined the photocatalytic activities of the prepared films by measuring the decomposition of stearic acid (10 mM in ethanol) that was spin-coated on the films. A 50 W halogen lamp was used as a visible-light source and a 420-nm cut-off filter was used for selecting only visible light. The amount of stearic acid remaining on the film was quantitatively characterized using a Fourier-transform infrared (FT-IR) spectrophotometer (model DA8-12, Bomen, Canada). Optimized geometry of atoms, electronic band structures, and density of states (DOSs) were calculated by density functional theory (DFT) using the well-tested CASTEP code which is based on the plane-wave pseudopotential method [31]. The generalized gradient approximation (GGA) with gradient corrected functional Perdew–Burke–Ernzerhof (PBE) has been used throughout the calculation. The $2 \times 2 \times 1$ supercell of TiO_2 anatase structure was used for this theoretical study.

Table 1
Nitrogen sources and structural characteristics of undoped- and N-doped TiO_2 nanoparticles.

Sample	N source	Crystallite size (nm)	*d* spacing for (1 0 1) plane (Å)	BET surface area (m^2/g)
PT	–	11.2	3.51	105.76
NT1	NH_3 (gas)	11.5	3.50	106.82
NT2	NH_4OH (aq.)	16.4	3.51	94.38
NT3	NH_4OH (aq.)	17.0	3.51	89.76

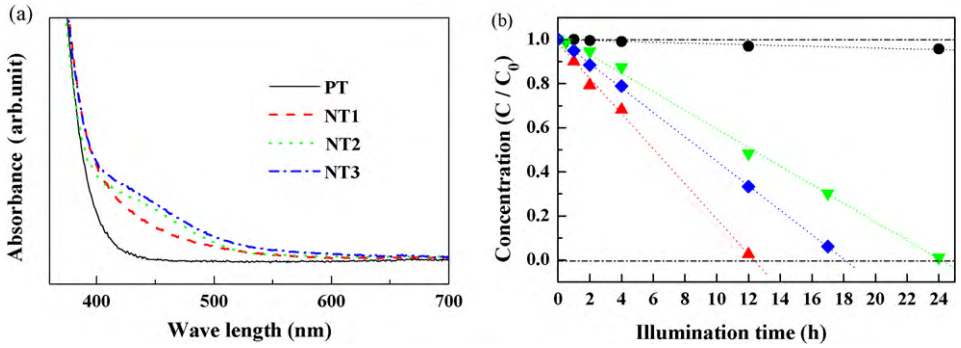

Fig. 2. (a) UV–vis diffuse-reflectance spectra of the synthesized nanoparticles and (b) concentration of phenol in the aqueous solution with presence of PT (●), NT1 (▲), NT2 (▼), and NT3 (◆) powders as a function of irradiation time ($\lambda \geq 420$ nm). The decrease of the concentration indicates the photocatalytic degradation of phenol. The degradation of phenol for the PT sample (3% in 12 h) can be attributed to the existence of some degree of visible light absorption up to 450 nm for PT (a).

3. Results and discussion

The crystal structures of the synthesized TiO_2 particles (PT, NT1, NT2, and NT3) were analyzed by using XRD technique. As shown in Fig. 1, all of the synthesized TiO_2 particles are pure anatase phase. XRD peaks were fitted by following the Debye–Scherrer equation and the crystallite size of the TiO_2 particles was calculated [32]. The crystallite size and other physical characteristics are summarized in Table 1. There is not any change in "*d*" space of (1 0 1) planes in four different powders, which indicates that the prepared nanoparticles possess similar crystallinity and that N is incorporated into the lattice without changing the average dimension of the unit cell [17]. The TEM micrographs (see Supplementary data 1) show that the nanoparticles have a fairly uniform spherical shape and that the crystallite sizes of the prepared nanoparticles are in the range of 10–20 nm, which is in agreement with the calculated crystallite sizes obtained from the XRD data. The BET surface area is in the range of 90–107 m^2/g. The difference in the surface area is consistent with the change in particle size.

The optical absorption characteristics and photocatalytic properties of the prepared samples are shown in Fig. 2a and b, respectively. Fig. 2a presents the diffuse-reflectance spectra of the N-doped and undoped TiO_2 powders. PT shows a small absorption tail over the region from 400 to 450 nm. In contrast, three different N doping methods significantly increase the absorption of visible light ranging from 400 to 550 nm. It is noted that NT1, NT2, and NT3 show different light absorption behaviors for the visible light. While the UV–vis spectrum of NT1 shows a tail-like feature with monotonous decrease in the absorption, the UV–vis spectrum of NT2 and NT3 show humps with a local peak of 450 nm. Also,

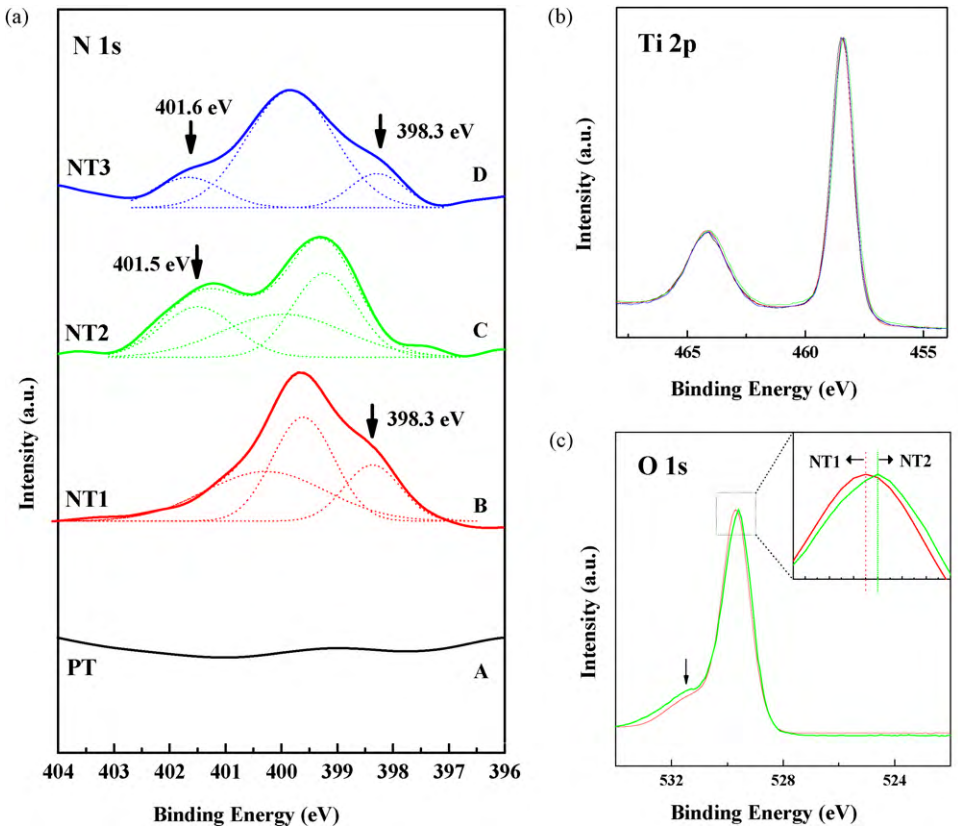

Fig. 3. XP spectra (solid lines) of the synthesized nanoparticles at the N 1s (a), Ti 2p (b), and O 1s (c) core levels. The dotted lines in (a) are the fitting curves of each XP spectrum. An arrow in (C) denotes the O 1s peak at 531.5 eV.

the absorbance of NT1 in the visible light region (400–550 nm) is lower than those of NT2 and NT3. The photocatalytic activity of TiO_2 nanoparticles over the visible light is remarkably improved when nitrogen is doped. After 12 h reaction, the remaining amount of phenol is 0.03% for NT1, 48% for NT2, and 33% for NT3 (see Fig. 2b). In contrast, more than 97% of phenol was still left in PT, which reveals that the doped nitrogen promotes the generation of radical ions by collecting photons in the visible light. The TOC analysis showed the consistent result. 99.5%, 54.1%, 69.3%, and 67.6% of carbon remained for PT, NT1, NT2, and NT3, respectively, after 12 h reaction. In three N-doped TiO_2 samples, differences in the degradation rates are observed. Though the crystallinity, particle size, and optical absorption of NT2 and NT3 are similar, NT3 has better photocatalytic activity than NT2. Moreover, NT1 absorbing less visible light shows better photocatalytic activity than NT2 and NT3. These experimental observations indicate that the amount of the visible light absorbed by N-doped TiO_2 is not only a factor determining the photocatalytic ability of N-doped TiO_2. To find out the origin of the different photocatalytic activity, the optical properties and the states of doped N were analyzed. The UV–vis data were converted to $[(\alpha h\nu)^{1/2}$ vs. $E]$, which were subsequently extrapolated [33], as shown in Supplementary data 2. The band gap energy of PT and NT2 is 3.00 eV, and that of NT1 and NT3 is 2.91 eV. It is remarkable that the extrapolation of the shoulder-like region for NT2 and NT3 indicates the charge transition energy of approximately 1.85 eV. The different optical characteristics of three different N-TiO_2 samples imply that each sample possess the different energy states, which may be caused by the different types of N doping. From the density of states (DOSs) calculations, Asahi et al. [2] has shown that substitutional N doping would narrow the band gap by the coupling of the O 2p and N 2p orbitals, while interstitial doping would create an additional defect state between the conduction band and valence band. Following studies [19,23,34] also reported that nitrogen impurities would induce the formation of localized states in the band gap and that the substitutional N states are present slightly above the valence band edge (0.14 eV). The energy state of interstitial N was proposed to 0.73 eV larger than the top of the valence band, which yields a new absorption band such as a shoulder-like absorption tail [23,35]. As a result, the interstitial N impurities work as hole trapping sites and reduce the direct oxidation power of N-TiO_2 in the photocatalytic process by decreasing the concentration of radical ions [2,23]. Therefore, the charge transition energy of about 1.85 eV in NT2 and NT3 samples indicates the inconsistency between the visible-light absorption characteristics and the photocatalytic activity can be correlated with the different N doping states of different N-TiO_2 samples.

Table 2
Nitrogen concentration of N-doped TiO_2 ($TiO_{2-x}N_x$) nanoparticles. The values refer to x calculated from the N 1s spectra shown in Fig. 3a.

Sample	N 1s total	400 eV	401.5 eV	398.3 eV
PT	–	–	–	–
NT1	0.0134	0.0107	–	0.0027
NT2	0.0143	0.0106	0.0037	–
NT3	0.0150	0.0110	0.0018	0.0022

The binding energy of N in N-TiO_2 nanoparticles were analyzed by using XPS. Fig. 3 shows the XP spectra of the N 1s, Ti 2p, and O 1s regions of the samples. The N-doped samples exhibit different N 1s peaks, which are fitted by using 2 or 3 subpeaks (Fig. 3a). The Ti 2p spectra of all samples are almost same (Fig. 3b). The N concentrations are listed in Table 2. The concentration was estimated by comparing product of integrated N 1s peak area and the nitrogen sensitivity factor (0.42) with product of integrated O 1s peak area (530 eV) and oxygen sensitivity factor (0.66). Three types of peaks, plotted from fitting curves, are observed at 398.3, 401.5, and approximately 400 eV, respectively. Among them, a peak with the binding energy (BE) of 400 eV is found in all of the N-doped samples with similar concentrations (about $x = 0.011$). In most of previous studies, this peak at 400 eV has been assigned to molecularly adsorbed or interstitially doped N species [2,9,12,18,28] such as NO_x and NH_x [1,9,29,30].

The BE peak at 398.3 eV is found in NT1 and NT3, and the BE peak at 401.5 eV is found in NT2 and NT3. N in TiN or simple chemisorbed N show the BE peak at ≤397.5 eV [17,27]. Therefore, the peak at 398.3 eV corresponds to N that has a lower electron density than the N present in the N–Ti–N structure. Because molecularly adsorbed N species appear at around 400 eV, the peak at 398.3 eV must correspond to N incorporated into the TiO_2 lattice in some manner. It is known that NO and NO_2 species appear above

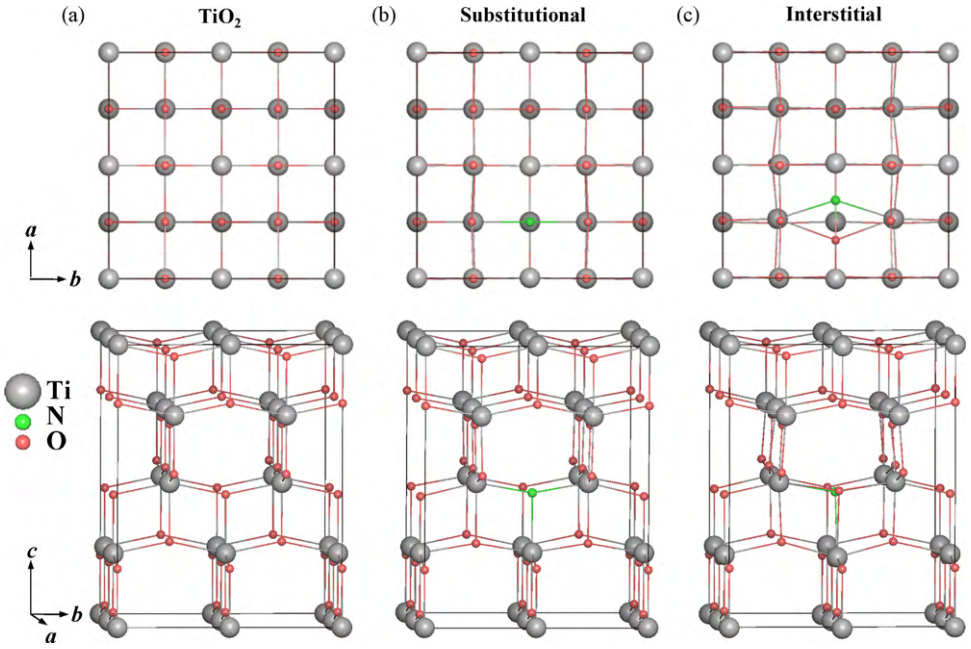

Fig. 4. The structural model of the $2 \times 2 \times 1$ TiO_2 anatase supercell (a) and the supercells containing substitutional N (b) and interstitial N (c).

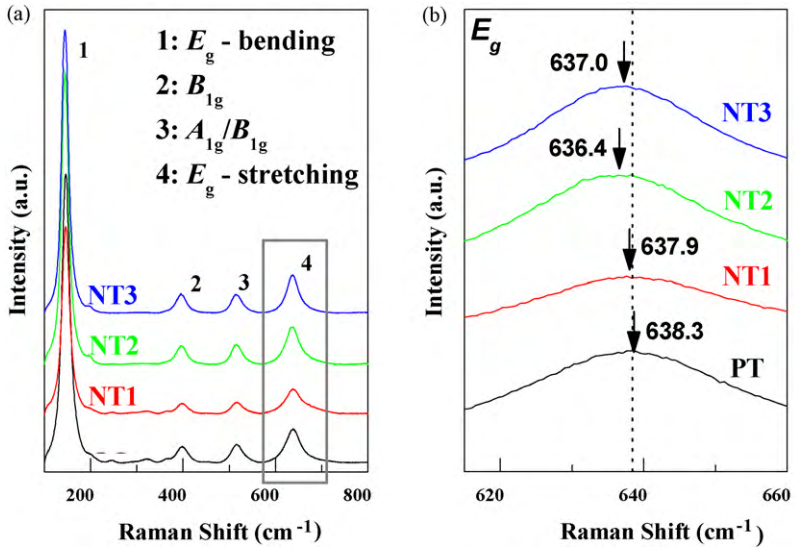

Fig. 5. Raman spectra of the synthesized nanoparticles (a), and the Raman spectra of E_g, the Ti–O stretching mode (b). The center of the E_g peaks are indicated by arrows and the values are noted in (b).

400 eV [18,29,36–39], hence we assign the N 1s peak at 398.3 eV to the anionic N^- in N–Ti–O linkages. Sathish et al. [17] and Ma et al. [28] found the N 1s peak at 398.2 and 398.3 eV, respectively. They also attributed these peaks to N^- in the N–Ti–O structure. The possibility of NH_3 being incorporated is ruled out, due to its higher BE (398.8 eV [20]), as reported by Sathish et al. [17]. The arguments in the above suggest that the 398.3 eV peak results from the N species which substitutes for O in the TiO_2 lattice as N–Ti–O.

Since the N 1s BE of substitutional N appears at 398.3 eV, the peak at 401.5 eV must be due to the different doping state of N that has a lower electron density than N in the form of N–Ti–O linkages. When N is incorporated into the TiO_2 lattice as Ti–O–N, the electron density of the oxidized N is lowered compared to that of N in the N–Ti–O structure and the BE of the 1s electron for oxidized N shifts to higher energy. Burda et al. indicated that the BE of the N 1s electron is higher as the formal charge of N becomes more positive (e.g., 408 eV in $NaNO_3$), as compared to N with zero or negative formal charge (398.8 eV in NH_3) [20,40]. Hence, the peak at 401.5 eV in this study is attributed to the N 1s level of oxidized N which has a configuration of Ti–O–N in the TiO_2 lattice, i.e. interstitial N doping [4,21–24,41]. When N is directly bonded to O, N also has connections with Ti and O to complete its valency [24].

In this study, the O 1s peaks are observed at 531.5 eV and 530 eV for both NT1 and NT2, as shown in Fig. 3c. However, the intensity ratio of the peaks at 531.5–530 eV is quite different. The peak of NT2 at 531.5 eV is higher than that of NT1. Although TiO_2 nanoparticles usually show the O 1s peak at 531.5 eV due to its contamination, such as OH^- (shown in Supplementary data 3), NT2 shows a higher peak at 531.5 eV than NT1, and this supports the presence of oxidized N species such as Ti–O–N being present [18,20,39]. Furthermore, it is noticeable that the 530 eV peak of NT2 is shifted to a lower BE compared to NT1 (the inset of Fig. 3c). The lower BE indicates that the higher electron density of O in NT2, that is the lower oxidation state of O in NT2 [20,39]. As O nearby an interstitial N is in a more reduced state than O nearby a substitutional N, this feature further confirms that N in NT2 is incorporated as Ti–O–N.

Based on the overall results of XP and UV–vis spectroscopic study, we attributed the 398.3 eV peak of NT1 and NT3 to substitutional N in an N–Ti–O structure, and the 401.5 eV peak of NT2 and NT3 to interstitial N in an Ti–O–N structure. Our synthetic methods and procedures for NT1, NT2, and NT3 are quite different from those of Sathish et al. [17], Ma et al. [28], or Burda et al. [4]. However, NT1 and NT3 have an N 1s peak at 398.3 eV that is very similar to those found by Sathish et al. [17] (398.2 eV) and Ma et al. [28] (398.3 eV); NT2 and NT3 have an N 1s peak at 401.5 eV that is also very close to that found by Burda et al. [4] (401.3 eV). Therefore, it is clear that different preparation routes can lead to different N 1s states in TiO_2. However, this does not imply that the electron BE of substitutional or interstitial N is dependent on the preparation route, but that different preparation routes can lead to different states of nitrogen in the TiO_2 crystalline structure.

Detailed atomic structures of N-TiO_2 lattices described above are theoretically calculated and schematically presented in Fig. 4. When the nitrogen impurities incorporate into TiO_2 crystalline, the Ti–O bond length of the structure could be varied, as different ionic radius and electron negativity between nitrogen and oxygen would deform the local balance constructed by Ti–O. Therefore, the distorted structures of the N-doped TiO_2 were estimated by using a geometry optimization with the CASTEP package, which is followed by the calculation of the electronic structure for the optimized geometry. A Nitrogen atom was placed in an oxygen atom site for the substitutional N-doped TiO_2, and a nitrogen atom was bonded with oxygen atoms for the interstitial N-doped TiO_2. As shown in Fig. 4a–c, the super cell of substitutional N-doped TiO_2 and interstitial N-doped TiO_2 deviate from the super cell of undoped anatase TiO_2. The average Ti–O bond lengths for the optimized structures of undoped TiO_2, substitutional N-doped TiO_2, and interstitial N-doped TiO_2 were 1.950 Å, 1.952 Å, and 1.961 Å, respectively. The large extension of the Ti–O bond length by the interstitial N doping indicates that there exists strong local strain energy. The changes in the local energy might affect the force constant of the bonds, which would influence the vibration frequency of the lattices. Therefore, Raman shift spectra of the PT, NT1, NT2, and NT3 were measured (Fig. 5) and compared with the results of the geometry optimization simulations. All the samples show the typical Raman shift spectra of TiO_2 anatase, as shown in Fig. 5a; about 144 (E_g, O–Ti–O bending mode, region 1), 400 (B_{1g}, region 2), 514 (A_{1g}/B_{1g}, region 3), and 639 cm^{-1} (E_g, Ti–O bond stretching mode, region 4) [42]. Since stretching wave numbers are related to the force constants and lengths of the bonding, Raman spectroscopic analysis can provide important information on the Ti–O bond lengths of the N-doped TiO_2 crystallines [43]. The best known empirical equations between stretching wave numbers (ν) and equilibrium bond lengths (R) are

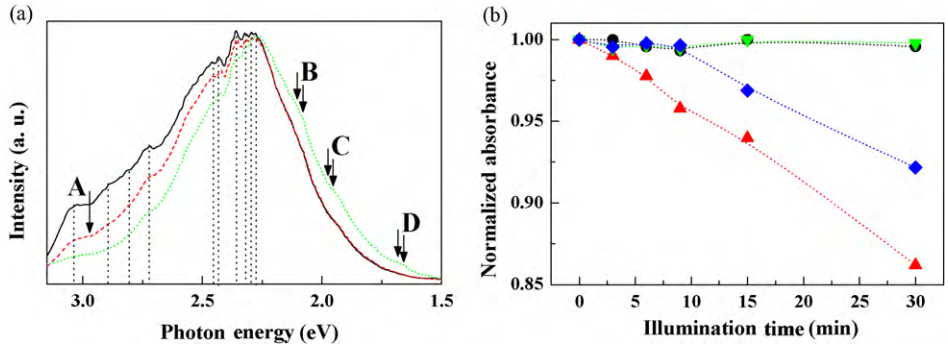

Fig. 6. (a) PL spectra of PT (solid), NT1 (– – –), and NT2 (- - - -) at 6 K. (b) Normalized absorbance of stearic acid on PT (●), NT1 (▲), NT2 (▼), and NT3 (◆) films as a function of irradiation time ($\lambda \geq 420$ nm). The decrease of the normalized absorbance indicates the photocatalytic degradation of stearic acid.

as follows:

$$\nu = A\exp(-BR) \quad \text{or} \quad \nu = A - BR$$

where A and B are experimentally derived fitting parameters [44,45]. Therefore, the significant red shift of the E_g peak (the stretching vibration mode of Ti–O), from 638.3 cm^{-1} (PT) to 636.4 cm^{-1} (NT2), can be attributed to the increase in Ti–O bond length, which is consistent with the results from the optimized structure. Also, corresponding to the estimated Ti–O bond length of the substitutional N-doped TiO_2 by geometry optimization, relatively less shift in wave number occurred for NT1 (637.9 cm^{-1}), that is, Ti–O bond length decreased more slightly. Therefore, the Raman spectra and the geometry optimization simulations provide an additional evidence for the different states of nitrogen in N-TiO_2. Moreover, the DOSs for the doped- and undoped-TiO_2 shown in Supplementary data 4 confirm that the interstitial doping induces an additional defect states between the conduction band and valence band in deeper region (1.05 and 0.52 eV, energy difference from valence band edge) than the substitutional doping (just narrowed band gap), which is consistent with the results from UV–vis spectrum shown in Fig. 2a and the previous reports [2,46].

The defect energy levels of PT, NT1, and NT2 were characterized by PL spectroscopy and the results are shown in Fig. 6a . All of the samples exhibit relatively shallow levels that are usually detected in the PL spectrum of anatase TiO_2 [47–49]. However, some differences in each sample are observed and the conceivable peaks are indicated in Fig. 6a as A to D. The peak of NT1 in region A assigned for indirect transitions, namely, $X1 \rightarrow \Gamma 1$ and $X2 \rightarrow \Gamma 1$ [47], shifted to a lower energy level compared to that in the spectra of PT. However, there is no difference between the spectra of PT and NT1 except for the shift in the phosphorescence peak region (region A, from 3.03 to 2.97 eV). These results are consistent with the narrowed optical band gap energy shown in Fig. 2a. On the other hand, NT2 shows distinct peaks in relatively deep levels marked as B (2.12–2.08 eV), C (1.99–1.95 eV), and D (1.69–1.65 eV). It is consistent with the results from UV–vis spectrum shown in Fig. 2a and the previous reports [2,46]. Finazzi et al. reported that interstitial nitrogen generates energy states at deep levels (0.41–1.44 eV) [46]. Moreover, our calculation results using DFT (Supplementary data 4) also present that interstitial nitrogen induces the deep defect energy levels, while substitutional nitrogen narrows the band gap. Even though the distinct energy levels, which were observed in the present PL study, cannot be exactly assigned to such calculated defect levels, the undefined energy levels of NT2 can be considered as defect levels associated with the interstitial N doping. In order to examine the effect of the interstitial N on the photocatalytic activities, films were made from three N-TiO_2 samples and stearic acid was spin-coated on the top of the films. While the photodecomposition of phenol occurs on the surface of the nanoparticles, the reaction with the stearic acid happens on the top of the film system. Hence, the holes generated in the middle or bottom of the films must be transferred onto the surface of the N-TiO_2 film to contribute to the photodecomposition of organic molecules. This indicates that the transport of the carriers becomes more important in the photocatalysis of the films. Therefore, if the interstitial N of NT2 traps the holes during their transport, a difference in the photocatalytic efficiency between films and powders becomes more pronounced in NT2, compared with NT1 and NT3 that have less carrier trapping sites. Fig. 6b shows the degradation of stearic acid on the N-TiO_2 films using visible light. Compared with the powder experiments (Fig. 2b), it is noted that the photocatalytic power of NT2 decreases significantly in the film experiments. Since the NT2 sample exhibited photocatalytic activity in the powder system (see Fig. 2b), the very low decomposition activity of NT2 film shown in Fig. 6b indicates that NT2 has more hole trapping sites preventing the transport of the holes from the middle or bottom of the films to the surface of N-TiO_2 films, leading to the decrease in the photocatalytic activity.

4. Conclusions

We found the N 1s binding energy peaks at 398.3, 401.5, and around 400 eV in the N-TiO_2 samples (NT1, NT2, and NT3) that were synthesized using different preparation methods. The optical absorption properties and photocatalytic activities of the three types of N-TiO_2 nanoparticles were obviously different in the presence of visible light. The difference in the optical absorption and photocatalytic activities was attributed to the different states of nitrogen present in each sample. From the XPS analysis, we attributed the 398.3 eV peak of NT1 and NT3 to substitutional N in an N–Ti–O structure, and the 401.5 eV peak of NT2 and NT3 to interstitial N in an Ti–O–N structure. The extended Ti–O bond length for NT2, confirmed by Raman spectra and the geometric optimization, was another evidence for the interstitially incorporation of nitrogen in NT2 nanocrystalline. The optical absorption spectra, DOSs calculated using DFT and PL measurements support the hypothesis that interstitial N doping creates defect levels in deep region of the band gap and that these defects disturb the charge transfer in the TiO_2 nanoparticles, in spite of the visible light absorption. A comparison of the photocatalytic decomposition in the powders and films show that the photocatalysis under visible light is more efficient for substitutional N doping than interstitial N doping due to smaller concentration of trapping sites.

Acknowledgements

This work was supported by WCU (World Class University) program through the Korea Science and Engineering Foundation

funded by the Ministry of Education, Science and Technology (R31-2008-000-10075-0). Kookmin Univ. portion was also supported by the Korea Research Foundation (KRF) grant funded by the Korea government (MEST) (2009-0065889 and R01-2008-000-20581-0). This work is also supported by the research program 2009 of Kookmin University in Korea.

Appendix A. Supplementary data

Supplementary data associated with this article can be found, in the online version, at doi:10.1016/j.jphotochem.2010.05.011.

References

[1] S. Sato, Photocatalytic activity of NO_x-doped TiO_2 in the visible-light region, Chem. Phys. Lett. 123 (1986) 126–128.
[2] R. Asahi, T. Morikawa, T. Ohwaki, K. Aoki, Y. Taga, Visible-light photocatalysis in nitrogen-doped titanium oxides, Science 293 (2001) 269–271.
[3] Z. Zou, J. Ye, K. Sayama, H. Arakawa, Direct splitting of water under visible light irradiation with an oxide semiconductor photocatalyst, Nature 414 (2001) 625–627.
[4] J.L. Gole, J.D. Stout, C. Burda, Y. Lou, X. Chen, Highly efficient formation of visible light tunable $TiO_{2-x}N_x$ photocatalysts and their transformation at the nanoscale, J. Phys. Chem. B 108 (2004) 1230–1240.
[5] M. Miyauchi, A. Ikezawa, H. Tobimatsu, H. Irie, K. Hashimoto, Zeta potential and photocatalytic activity of nitrogen doped TiO_2 thin films, Phys. Chem. Chem. Phys. 6 (2004) 865–870.
[6] J.M. Mwabora, T. Lindgren, E. Avendano, T.F. Jaramillo, J. Lu, S.E. Lindquist, C.G. Granqvist, Structure, composition, and morphology of photoelectrochemically active $TiO_{2-x}N_x$ thin films deposited by reactive DC magnetron sputtering, J. Phys. Chem. B 108 (2004) 20193–20198.
[7] M. Kitano, K. Funatsu, M. Matsuoka, M. Ueshima, M. Anpo, Preparation of nitrogen-substituted TiO_2 thin film photocatalysts by the radio frequency magnetron sputtering deposition method and their photocatalytic reactivity under visible light irradiation, J. Phys. Chem. B 110 (2006) 25266–25272.
[8] O. Diwald, T.L. Thompson, E.G. Goralski, S.D. Walck, J.T. Yates, The effect of nitrogen ion implantation on the photoactivity of TiO_2 rutile single crystals, J. Phys. Chem. B 108 (2004) 52–57.
[9] O. Diwald, T.L. Thompson, T. Zubkov, E.G. Goralski, S.D. Walck, J.T. Yates, Photochemical activity of nitrogen-doped rutile TiO_2(1 1 1) in visible light, J. Phys. Chem. B 108 (2004) 6004–6008.
[10] M. Batzill, E.H. Morales, U. Diebold, Influence of nitrogen doping on the defect formation and surface properties of TiO_2 rutile and anatase, Phys. Rev. Lett. 96 (2006) 026103.
[11] C. Burda, Y. Lou, X. Chen, A.C.S. Samia, J. Stout, J.L. Gole, Enhanced nitrogen doping in TiO_2 nanoparticles, Nano Lett. 3 (2003) 1049–1051.
[12] S. Sakthivel, M. Janczarek, H. Kisch, Visible light activity and photoelectrochemical properties of nitrogen-doped TiO_2, J. Phys. Chem. B 108 (2004) 19384–19387.
[13] S. Livraghi, A. Votta, M.C. Paganini, E. Giamello, The nature of paramagnetic species in nitrogen doped TiO_2 active in visible light photocatalysis, Chem. Commun. (2005) 498–500.
[14] Z. Lin, A. Orlov, R.M. Lambert, M.C. Payne, New insights into the origin of visible light photocatalytic activity of nitrogen-doped and oxygen-deficient anatase TiO_2, J. Phys. Chem. B 109 (2005) 20948–20952.
[15] S. Sato, R. Nakamura, S. Abe, Visible-light sensitization of TiO_2 photocatalysts by wet-method N doping, Appl. Catal. A 284 (2005) 131–137.
[16] Y. Nosaka, M. Matsushita, J. Nisino, A.Y. Nosaka, Nitrogen-doped titanium dioxide photocatalysts for visible response prepared by using organic compounds, Sci. Technol. Adv. Mater. 6 (2005) 143–148.
[17] M. Sathish, B. Viswanathan, R.P. Viswanath, C.S. Gopinath, Synthesis, characterization, electronic structure, and photocatalytic activity of nitrogen-doped TiO_2 nanocatalyst, Chem. Mater. 17 (2005) 6349–6353.
[18] N.C. Saha, H.G. Tompkins, Titanium nitride oxidation chemistry: an X-ray photoelectron spectroscopy study, J. Appl. Phys. 72 (1992) 3072–3079.
[19] H. Irie, Y. Watanabe, K. Hashimoto, Nitrogen-concentration dependence on photocatalytic activity of $TiO_{2-x}N_x$ powders, J. Phys. Chem. B 107 (2003) 5483–5486.
[20] X. Chen, C. Burda, Photoelectron spectroscopic investigation of nitrogen-doped titania nanoparticles, J. Phys. Chem. B 108 (2004) 15446–15449.
[21] X. Chen, T.-B. Lou, A.C.S. Samia, C. Burda, J.L. Gole, Formation of oxynitride as the photocatalytic enhancing site in nitrogen-doped titania nanocatalysts: comparison to a commercial nanopowder, Adv. Funct. Mater. 15 (2005) 41–49.
[22] S.M. Prokes, J.L. Gole, X. Chen, C. Burda, W.E. Carlos, Defect-related optical behavior in surface-modified TiO_2 nanostructures, Adv. Funct. Mater. 15 (2005) 161–167.
[23] C.D. Valentin, G. Pacchioni, A. Selloni, S. Livraghi, E. Giamello, Characterization of paramagnetic species in N-doped TiO_2 powders by EPR spectroscopy and DFT calculations, J. Phys. Chem. B 109 (2005) 11414–11419.
[24] C. Burda, J. Gole, Reply to "comment on photoelectron spectroscopic investigation of nitrogen-doped titania nanoparticles", J. Phys. Chem. B 110 (2006) 7081–7082.
[25] J.S. Jang, H.G. Kim, S.M. Ji, S.W. Bae, J.H. Jung, B.H. Shon, J.S. Lee, Formation of crystalline $TiO_{2-x}N_x$ and its photocatalytic activity, J. Solid State Chem. 179 (2006) 1067–1075.
[26] B. Gao, Y. Ma, Y. Cao, W. Yang, J. Yao, Great enhancement of photocatalytic activity of nitrogen-doped titania by coupling with tungsten oxide, J. Phys. Chem. B 110 (2006) 14391–14397.
[27] Y. Cong, J. Zhang, F. Chen, M. Anpo, Synthesis and characterization of nitrogen-doped TiO_2 nanophotocatalyst with high visible light activity, J. Phys. Chem. C 111 (2007) 6976–6982.
[28] T. Ma, M. Akiyama, E. Abe, I. Imai, High-efficiency dye-sensitized solar cell based on a nitrogen-doped nanostructured titania electrode, Nano Lett. 5 (2005) 2543–2547.
[29] J.A. Rodriguez, T. Jirsak, J. Dvorak, S. Sambasivan, D. Fischer, Reaction of NO_2 with Zn and ZnO: Photoemission, XANES, and density functional studies on the formation of NO_3, J. Phys. Chem. B 104 (2000) 319–328.
[30] Y. Sakatani, J. Nunoshige, H. Ando, K. Okusako, H. Koike, T. Takata, J.N. Kondo, M. Hara, K. Domen, Photocatalytic decomposition of acetaldehyde under visible light irradiation over La^{3+} and N co-doped TiO_2, Chem. Lett. 32 (2003) 1156–1157.
[31] M.D. Segall, P.J.D. Lindan, M.J. Probert, C.K. Pickard, P.J. Hasnip, C.J. Clark, M.C. Payne, First-principles simulation: ideas, illustrations and the CASTEP code, J. Phys.: Condens. Matter. 14 (2002) 2717–2744.
[32] B.D. Cullity, Elements of X-ray Diffraction, Addision-Wesley, Reading, MA, 1987.
[33] N. Serpone, D. Lawless, R. Khairutdinov, Size effects on the photophysical properties of colloidal anatase TiO_2 particles: size quantization versus direct transitions in this indirect semiconductor? J. Phys. Chem. 99 (1995) 16646–16654.
[34] R. Nakamura, T. Tanaka, Y. Nakato, Mechanism for visible light responses in anodic photocurrents at N-doped TiO_2 film electrodes, J. Phys. Chem. B 108 (2004) 10617–10620.
[35] D. Li, N. Ohashi, S. Hishita, T. Kolodiazhnyi, H. Haneda, Origin of visible-light-driven photocatalysis: a comparative study on N/F-doped and N–F-codoped TiO_2 powders by means of experimental characterizations and theoretical calculations, J. Solid State Chem. 178 (2005) 3293–3302.
[36] N.D. Shinn, K.-L. Tsang, Strain-induced surface reactivity—low-temperatuce Cr/W(1 1 0) nitridation, J. Vac. Sci. Technol. A 9 (1991) 1558–1562.
[37] S. Sugai, H. Watanabe, T. Kioka, H. Miki, K. Kawasaki, Chemisorption of NO on Pd(1 0 0), (1 1 1) and (1 1 0) surfaces studied by AES, UPS and XPS, Surf. Sci. 259 (1991) 109–115.
[38] D.R. Rainer, S.M. Vesecky, M. Koranne, W.S. Oh, D.W. Goodman, The CO + NO reaction over Pd: a combined study using single-crystal, planar-model-supported, and high-surface-area Pd/Al_2O_3 catalysts, J. Catal. 167 (1997) 234–241.
[39] E. Gyorgy, A. Perez del Pino, P. Serra, J.L. Morenza, Depth profiling characterisation of the surface layer obtained by pulsed Nd:YAG laser irradiation of titanium in nitrogen, Surf. Coat. Technol. 173 (2003) 265–270.
[40] NIST/EPA Gas-Phase Infrared Database, http://webbook.nist.gov/chemistry/, http://srdata.nist.gov/xps/.
[41] C.S. Gopinath, Comment on "photoelectron spectroscopic investigation of nitrogen-doped titania nanoparticles", J. Phys. Chem. B 110 (2006) 7079–7080.
[42] T. Ohsaka, F. Izumi, Y. Fujiki, Raman-spectrum of anatase, TiO_2, J. Raman Spectrosc. 7 (1978) 321–324.
[43] L. Popovic, D. de Waal, J.C.A. Boeyens, Correlation between Raman wave numbers and P–O bond lengths in crystalline inorganic phosphates, J. Raman Spectrosc. 36 (2005) 2–11.
[44] F.D. Hardcastle, I.E. Wachs, Determination of niobium–oxygen bond distances and bond orders by Raman spectroscopy, Solid State Ionics 45 (1991) 201–213.
[45] G.D. Chryssikos, Bond length–Raman frequency correlations in borate crystals, J. Raman Spectrosc. 22 (1991) 645–650.
[46] E. Finazzi, C.D. Valentin, A. Selloni, G. Pacchioni, First principles study of nitrogen doping at the anatase TiO_2(1 0 1) surface, J. Phys. Chem. C 111 (2007) 9275–9282.
[47] N. Daude, C. Gout, C. Jouanin, Electronic band structure of titanium dioxide, Phys. Rev. B 15 (1977) 3229–3235.
[48] N.D. Abazović, M.I. Čomor, M.D. Dramićanin, D.J. Jvanović, S.P. Ahrenkiel, J.M. Nedeljković, Photoluminescence of anatase and rutile TiO_2 particles, J. Phys. Chem. B 110 (2006) 25366–25370.
[49] V. Melnyk, V. Shymanovska, G. Puchkovska, T. Bezrodna, G. Klishevich, Low-temperature luminescence of different TiO_2 modifications, J. Mol. Struct. 744 (2005) 573–576.